Journal of Power Sources 245 (2014) 678–683

Contents lists available at SciVerse ScienceDirect

Journal of Power Sources

journal homepage: www.elsevier.com/locate/jpowsour

Short communication

Spatially resolved in operando neutron scattering studies on Li-ion batteries

A. Senyshyn [a,*], M.J. Mühlbauer [a,b], O. Dolotko [a,b], M. Hofmann [a], T. Pirling [c], H. Ehrenberg [d]

[a] Forschungs-Neutronenquelle Heinz Maier-Leibnitz FRM II, Technische Universität München, Lichtenbergstraße 1, D-85748 Garching b. München, Germany
[b] Material Science, Technische Universität Darmstadt, Petersenstrasse 23, D-64287 Darmstadt, Germany
[c] Institut Laue-Langevin, 6 rue Jules Horowitz, Grenoble Cedex 9 BP 156-38042, France
[d] Karlsruhe Institute of Technology (KIT), Institute for Applied Materials (IAM-ESS), Hermann-von-Helmholtz-Platz 1, D-76344 Eggenstein-Leopoldshafen, Germany

HIGHLIGHTS

- In operando spatially resolved neutron powder diffraction.
- Probe of spatial lithium distribution in both cathode and anode.
- Both fresh and degraded cells studied have spatially uniform lithium distribution.
- Details of Li-ion battery design deduced using neutron radiography and tomography.
- Advantages of using monochromatic neutron beam for studies of lithium distribution.

GRAPHICAL ABSTRACT

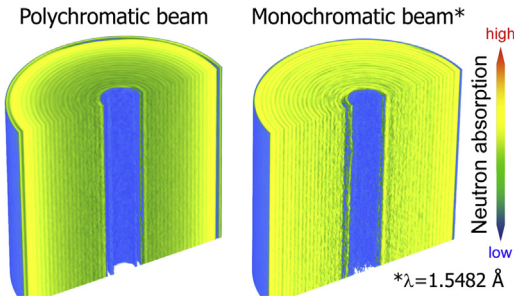

ARTICLE INFO

Article history:
Received 23 April 2013
Received in revised form
14 June 2013
Accepted 21 June 2013
Available online 5 July 2013

Keywords:
Li-ion battery
In operando studies
Fatigue effect
Spatial lithium distribution
Neutron powder diffraction
Neutron radiography and tomography

ABSTRACT

Spatially-resolved neutron diffraction has been applied to probe the lithium distribution in radial direction of a commercial Li-ion cell of 18650-type. The spatial evolution of selected Bragg reflections for $LiCoO_2$ (positive electrode, "cathode") and graphite and lithium intercalated graphite (negative electrode, "anode") was observed and evaluated by taking beam attenuation and cell geometry effects into account. No evidences for lithium inhomogeneities have been found for the investigated set of cells. Computed neutron tomography using a monochromatic neutron beam confirmed the homogeneous lithium distribution. The relevance of the monochromatic beam to neutron imaging studies of Li-ion cells is discussed.

Li-ion batteries are considered as the major energy storage technology in the field of portable electronics and electric vehicles. Applications in electromobility demand for rechargeable batteries with higher energy density, improved output power, lower weight and lower costs. These performance parameters are determined by numerous degrees of freedom, from chemical and structural details of the used materials up to the cell design and processing. An optimization of such complicated electrochemical devices requires "live" information about processes occurring inside the cell. This

* Corresponding author.
E-mail addresses: anatoliy.senyshyn@gmail.com, anatoliy.senyshyn@frm2.tum.de (A. Senyshyn).

0378-7753/$ – see front matter © 2013 Elsevier B.V. All rights reserved.
http://dx.doi.org/10.1016/j.jpowsour.2013.06.158

calls for new dedicated experimental techniques, which are non-destructive and capable to study complete operational cells without a need to disassemble them. Hereby, the risks of material oxidation, electrolyte evaporation or uncontrolled changes of the state of charge are minimized. Furthermore, 3D information on cell components on different length scales is of high relevance. Neutron scattering is already a well established tool for the characterization of complex Li-ion batteries [1]. The major advantageous features are: (1) the high penetration depths of thermal neutrons, which suits perfectly for non-destructive studies on complete devices, (2) the capability to localize light elements, e.g. hydrogen, lithium, (3) the excellent phase contrast depending on specific isotopes and complementary to the X-ray absorption contrast, (4) the interaction with nuclei, so that the neutron scattering lengths are not dependent on $\sin(\theta)/\lambda$, and accurate structure factors can be measured over a broad range of diffraction angles. Such data sets provide precise bond-lengths and allow Debye–Waller factor analysis along with the direct determination of lithium diffusion pathways by probability density function analysis. Therefore, numerous neutron scattering studies of Li-ion cells have been performed. The evolution of polycrystalline electrode materials was revealed *in situ* by neutron powder diffraction [2–10]. The solid-electrolyte formation processes have been investigated by small angle neutron scattering [11] and neutron reflectometry [12]. Neutron imaging (especially computed neutron tomography) has been established as an excellent method for "live" studies (in operando) of the full cell design and the electrochemical behavior of Li-ion cells. These results are displayed by a 3D visualization of the local neutron attenuation contrast with a spatial resolution down to the range of several μm [13–16].

Recently reported computed neutron tomography studies on commercial Li-ion cells of the 18650-type [3] revealed a pronounced contrast between the electrode layers (rolled around a center pin) in the discharged state, which vanishes during cell charge. This effect is attributed to the inhomogeneous lithium distribution in the discharged state, when the major amount of lithium is situated inside the positive electrode ($LiCoO_2$) and the negative electrode (graphite) is nearly Li-free. The lithium intercalation into the negative electrode results in a more uniform lithium distribution between the electrodes (ideally, in the fully charged state LiC_6/LiC_{12} and $Li_{0.5}CoO_2$) reducing the contrast. In addition to this coherent interlayer contrast depending on the state of charge, a neutron attenuation gradient in radial direction has been observed which is affected neither by fatigue nor by the state-of-charge. It has also been attributed to the distribution of lithium inside the cell, corresponding to a scenario when more lithium is concentrated in the outer part of the cell. However, from the electrochemical point of view this situation with a non-uniform Li concentration is inconsistent with the homogeneous capacity expected from the equipotentials along the metal foil current collectors in commercial cells. This calls for an alternative technique capable to quantify the lithium distribution inside the Li-ion cell in operando. Spatially-resolved neutron diffraction is the method of choice for this task, but to our knowledge its application to energy storage systems with complicated geometries is limited so far to Fe/NaCl based batteries [17]. Just recently an *in situ* neutron diffraction study of the inhomogeneous degradation in a $Li_xMn_2O_4$/graphite-based commercial pouch-cell battery has been reported [18].

Nevertheless, in addition to the quantification of lithium uniformity of the following conceptual questions still have to be answered:

- Is it possible to obtain and evaluate the spatially-resolved diffraction signal from a highly neutron-absorbing commercial cylindrical cell of the 18650-type?
- What is the influence of discrete electrode layers on the diffraction signal, and which gauge volume is eligible? Or in other words: up to which extent can the rolled electrode layers be modeled as an isotropic medium?

A spatially-resolved neutron powder diffraction experiment can be performed at nearly any kind of engineering diffractometer equipped with translation and rotation stages for sample positioning and a suitable collimation. A sketch of such a setup is displayed in Fig. 1a. The shape of the gauge volume is defined by the collimation of the incident and scattered neutron beam and the

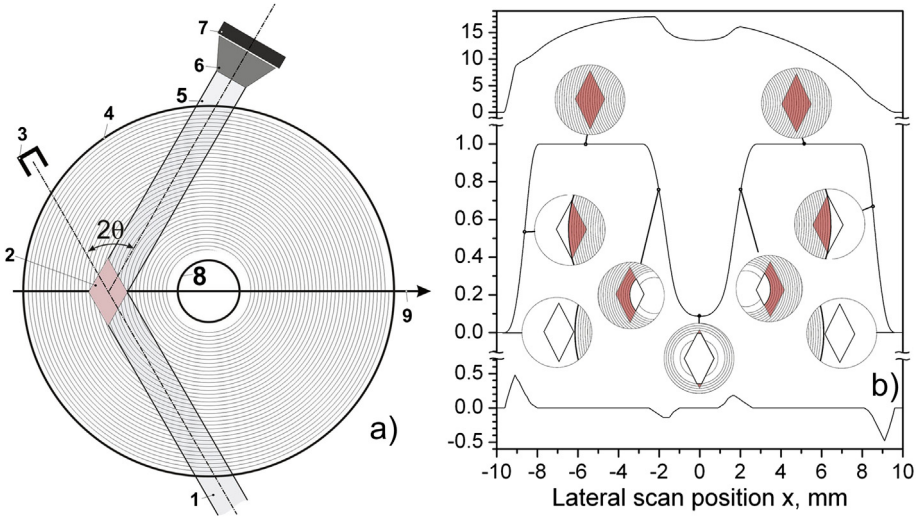

Fig. 1. (a) Sketch of spatially resolved neutron diffraction experiment on a cylindrical Li-ion cell, where 1 and 5 correspond to the incident and elastically scattered neutron beam, 2 is the gauge volume, 3 is the direct beam catcher, 4 and 8 are the cell housing and center pin, 6 is the oscillating radial collimator, 7 is the 2D neutron detector and 9 indicates the scanning direction *x*. The effective gauge volume, containing the actually scattering material, is marked by red color. (b) Typical dependencies of the neutron path length through the cylindrical cell (top, in mm), the fraction of the gauge volume filled with material (middle, relative units) and the resulting shift for the center of mass of the effective gauge volume (bottom, mm). The insets show the gauge volume for different positions of the lateral scan. (For interpretation of the references to color in this figure legend, the reader is referred to the web version of this article.)

scattering angle. By moving the sample with respect to the fixed gauge volume, a spatially-resolved scattering response from different sample sections can be obtained. Assuming an isotropic medium, the acquired diffraction data must be evaluated including beam attenuation and surface effects due to the sample geometry. On the first instance a cylindrical cell of the 18650-type can be approximated by two concentric cylinders with an absorbing and scattering medium in between. The outer cylinder corresponds to the steel housing and the inner one to the center pin. The values for the outer boundary R and inner boundary r of electrode materials differ slightly from the values determined from the housing and the center pin, for example due to an electronic isolation by additional separator layers. With given R and r the neutron path length L for an elastic neutron scattering process occurring at an angle 2θ and at position x within the cell can be calculated for every configuration on the basis of simple geometric considerations. Due to the curvature of the inner and outer surfaces the typical $L(x)$ profile (shown in Fig. 1b, top) has an asymmetric and nonlinear shape with a well resolved local minimum around $x = 0$ corresponding to an empty volume at the center pin. The complex dependency of the neutron path length on the position x gives rise to significant nonlinearities of the beam attenuation.

Furthermore, the two-cylinder geometry causes substantial boundary effects contributing to the diffraction signal. The situation at the surfaces (both inner and outer), where the physical volume of the scattering electrode material is less than the gauge volume, creates a noticeable reduction of the scattered signal. This effect as well as its consequences is well known and parameterized for flat surfaces [19], but to our knowledge no universal solution exists for more complicated geometries. Therefore, the intersection of the gauge volume and the scattering material has been evaluated using a spatial segmentation with a voxel size of 1 μm^3 (or approx. 0.01% in intensity). The typical correction factor for the intensity is symmetric around $x = 0$ and shown in Fig. 1b (middle) for different cases of boundary conditions. This factor has a substantial influence on the diffracted intensities, especially at the boundaries. It is highly dependent on the values of R and r as well as on the definition of the gauge volume (beam collimation). A change of the size and shape of the effective gauge volume, formed by the intersection of the gauge volume and the scattering material, during a lateral scan leads to a shift of the corresponding center of mass of the investigated cell volume. At the boundaries of the electrode materials the center of mass is shifted with respect to the central beam position. The sign of the shift depends on the surface configuration (see Fig. 1b, bottom). This shift will cause an overall displacement of the position of the Bragg reflections.

The spatially-resolved neutron diffraction experiment has been performed at the material science diffractometer STRESS-SPEC (FRM II, Garching b. München, Germany) [20]. Monochromatic neutrons with a wavelength of 1.645 Å have been selected from the germanium monochromator (Ge311) at a take-off angle of 57.4°. Lateral scans with a gauge volume of ca. $2 \times 2 \times 20$ mm^3 were performed using a slit for the incoming beam and a radial oscillating collimator for the scattered neutron beam. The z position of the cells was adjusted, so that the gauge volume was centered at the middle height of the cells. All experiments have been performed on previously investigated [3,4] commercial Li-ion cells. Three sequential charge/discharge cycles (constant current/constant voltage, 3.0–4.2 V, 0.4 A) have been performed for the determination of the actual electrochemical performance parameters, prior to the neutron studies on fully charged cells. The lateral scans were performed along the cell diameter over the range of −10 mm to +10 mm with respect to its center with a step width of 0.5 mm. The scan direction was defined as a bisecting line of the incoming and diffracted neutron beam (Fig. 1a).

Among the different Bragg reflections originating from the electrode materials of Li-ion cells the 001 LiC_6 and 002 LiC_{12} reflections are known to possess the highest structure factors. Due to the staging behavior of these intercalated carbons a change of the lithium concentration might be accompanied by a change of the intensity ratio between these two reflections, whilst their angular positions remain constant [21]. This fact makes them suitable candidates for probing the lithium uniformity in the negative electrode.

The 2D plot of the diffraction data (Fig. 2a) shows the logarithmic intensity in false-color representation collected over a 2θ range of 24°–29° vs. the lateral scan position, where $x = 0$ corresponds to the geometric center of the cylindrical Li-ion cell. The obtained diffraction data are highly affected by an offset of the gauge volume, e.g. at $x = \pm 10$, which is beyond the cell volume. Here nearly no elastic scattering signal has been observed. Hence, already a small shift towards the center ($x = 0$) results in a fast growth of the intensities of both reflections, 001 LiC_6 and 002 LiC_{12}. The intensities and positions of the reflections are represented by points in Fig. 2b and c, extracted from the experimental diffraction profile of each lateral scan position by a single profile decomposition, assuming a Gaussian peak shape.

Smooth, but highly nonlinear spatial dependencies of the reflection intensities have been obtained, where the evolution of 001 LiC_6 and 002 LiC_{12} reflections has been found to be very similar. Within the limits of data accuracy the intensity ratio of the considered LiC_6/LiC_{12} reflections remains unchanged during the lateral scans, which is a hint to a homogeneous lithium distribution over the cell volume. Beam attenuation and surface effects are included to simulate the observed lateral intensity profiles as mentioned before. Therefore, the linear attenuation coefficient μ can be extracted as well, which describes the slope of the intensity increase or decrease. The electrode dimensions R and r (8.75 and

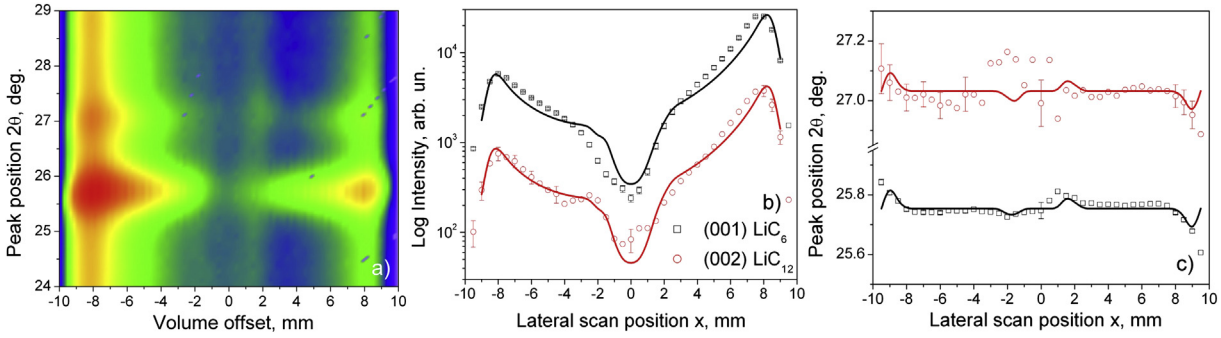

Fig. 2. Two-dimensional diffraction data obtained during a lateral scan (a) (logarithmic intensities are shown in the false-color representation) along with the intensities (b) and positions (c) of the 001/002 LiC_6/LiC_{12} doublet as extracted from the single profile decomposition of data collected on a fresh cell at STRESS-SPEC diffractometer ($2 \times 2 \times 20$ mm^3/sin2θ gauge volume). Solid lines denote values of a numerical model using the parameters listed in Table 1.

2 mm, respectively) have been determined from previous neutron imaging studies [3]. The best agreement between the observed and simulated lateral intensity profiles has been found with the parameters listed in lines 1–2 of Table 1 and the corresponding model is shown in Fig. 2b by solid lines. The observed deviations of 001 LiC_6 and 002 LiC_{12} diffraction angles shown in Fig. 2c can be explained by a shift of the center of mass in the gauge volume (solid line, simulated curves on the basis of *R*, *r*, resolution and sample to detector distance of 1050 mm). They are, therefore, considered as artifacts and do not reflect structural changes. The reflection positions remain actually constant, in agreement with the stage 1 and stage 2 structure models for LiC_6 and LiC_{12}, respectively.

The experimental results and their simulations indicate that the use of a $2 \times 2 \times 20$ mm^3 gauge volume is appropriate for a description of the obtained diffraction data within the isotropic attenuation approximation and geometrical restrictions. A test with a smaller gauge volume was performed at the SALSA engineering diffractometer (Institute Laue Langevin, Grenoble, France) [22]. The experimental setup was similar to the one used at STRESS-SPEC, and the most remarkable differences are (1) the primary beam collimation (use of an oscillating radial collimator instead of a simple slit) enabling a gauge volume of only $1 \times 1 \times 20$ mm^3, (2) the detector-to-sample distance of 1010 mm and (3) the use of a hexapod sample stage (Gough–Stewart platform) for the lateral scans. Due to the cylindrical cell symmetry the lateral scans have been performed in the 0–9.6 mm range using steps of 0.6 mm. In contrast to STRESS-SPEC data the improved spatial resolution causes a nearly undetectable intensity signal in the region of the center pin, where no electrode material is located. Therefore data in the range of 0–1.8 mm were not included in the further considerations and simulations. Due to the improved spatial resolution the radial scan data were corrected for an offset in scan direction *x* in order to compensate for some inaccuracy in the cell mounting and deviations from a perfect cylinder geometry.

In addition to 001/002 LiC_6/LiC_{12} reflections the evolution of the graphite 002 reflection (cell discharged to 3.0 V) has been analyzed with this setup. Experiments were carried out on a "fresh" cell and a "fatigued" cell, the latter after 1000 sequential CCCV cycles (1 C from 3.0 to 4.2 V) at 25 °C (see Ref. [4] for details). The decomposed diffraction profiles have been found consistent with the previous ones from STRESS-SPEC (Fig. 3): reflection intensities for graphite and lithium intercalated carbons evolve in the same way and the positions of the reflections are nearly independent on the spatial coordinate. A comparison of the spatial intensity profiles indicates a similar behavior for both fresh and fatigued cells, which suggests the stability of the attenuation coefficient during fatigue and, accordingly, of the overall cell chemical content. Conclusions about possible shifts of the reflections from lithium intercalated carbons are limited by the instrumental resolution [23]. Nevertheless, systematically lower diffraction angles of the carbon reflections are observed for the fatigued cell in comparison to the fresh cell. This shifts result from larger lattice parameters *c* of the carbon, consistent with some residual lithium, embedded in the graphite matrix [4]. Simulation of the obtained profiles yields scattered intensity I_s and attenuation coefficients μ for the different diffraction data and different states of health and fatigue (see Table 1, lines 3–8). The attenuation coefficients are determined on the basis of SALSA and STRESS-SPEC data for different Bragg reflections from the negative electrode. They are in fair agreement, whereas some deviations in the intensity ratios for the 001/002 LiC_6/LiC_{12} reflections have been noticed. The experiment at STRESS-SPEC yields a factor of 6.5 for the fresh cell, whereas a similar experiment at SALSA resulted in 3.24. Bearing in mind the identical state-of-charge for both cells the reason for this discrepancy can be related to the spatial resolution and the instrumental resolution function, but is not yet fully understood. The 001/002 LiC_6/LiC_{12} intensity ratio for the fatigued cell is even much lower (0.756). A reduction of this ratio is in agreement with the observed structural response of the negative electrode caused by aging [3,4].

No remarkable evidence for spatial inhomogeneities of the lithium distribution in the graphite negative electrode has been observed, but to complete a consistent pattern the positive electrode needs also to be addressed. Among different $LiCoO_2$ reflections, the 003 one is the most appropriate as it is well separated and has rather high intensity (ca. 15% of the strongest graphite reflection). In contrast to the previously considered LiC_6/LiC_{12} doublet, whose intensity ratio reflects the state-of-charge of the cell, the intensity of 003 $LiCoO_2$ remains nearly constant upon charge/discharge. However its diffraction angle is known to vary over a broad range due to a pronounced response of the lattice parameter *c* on Li intercalation/extraction in Li_xCoO_2. The spatial evolution of the 003 reflection parameters for Li_xCoO_2 is shown for both fresh and fatigued batteries in Fig. 4. The spatial intensity distributions in charged and discharged states and for two extremes of fatigue have been found very similar to the above-mentioned graphite behavior. Within the limits of experimental accuracy no remarkable spatial dependence can be concluded for the 003 $LiCoO_2$ diffraction angle, but its weak intensity dependence on lithium content does not allow reliable conclusions about the spatial homogeneity within the positive electrode material. Hence, a comparison of reflection positions for fresh and fatigued batteries indicate excellent agreement in the charged state, whereas in

Table 1
Parameters of the lateral intensity profile simulations/calculations and fit residuals for electrode materials studied at SALSA and STRESS-SPEC. The radii *R* and *r* determining the outer and inner limitation of the electrode materials were set to 8.75 and 2 mm, respectively.

Cell state		Instrument	Reflection	Mean peak position, deg. 2θ	Intensity I_s, arb. un.	Absorption coefficient μ, mm^{-1}	(COD)[a]
Fresh	Charged	STRESS-SPEC	001 LiC_6	25.75(2)	$6.83(3) \times 10^4$	0.212(2)	0.91921
Fresh	Charged	STRESS-SPEC	002 LiC_{12}	27.03(4)	$1.05(1) \times 10^4$	0.210(1)	0.85660
Fresh	Discharged	SALSA	002 C	28.39(3)	$4.88(4) \times 10^3$	0.210(1)	0.94472
Fresh	Charged	SALSA	001 LiC_6	25.78(2)	$3.80(7) \times 10^3$	0.211(1)	0.99560
Fresh	Charged	SALSA	002 LiC_{12}	27.04(5)	$1.17(4) \times 10^3$	0.215(1)	0.97485
Fatigued	Discharged	SALSA	002 C	28.30(2)	$3.88(8) \times 10^3$	0.214(3)	0.99283
Fatigued	Charged	SALSA	001 LiC_6	25.79(2)	$1.86(6) \times 10^3$	0.217(3)	0.93717
Fatigued	Charged	SALSA	002 LiC_{12}	27.10(2)	$2.46(1) \times 10^3$	0.206(1)	0.96800
Fresh	Discharged	SALSA	003 $LiCoO_2$	20.16(2)	$6.94(4) \times 10^2$	0.209(1)	0.95788
Fresh	Charged	SALSA	003 $LiCoO_2$	19.65(2)	$1.09(5) \times 10^3$	0.206(3)	0.85204
Fatigued	Discharged	SALSA	003 $LiCoO_2$	19.97(5)	$1.04(5) \times 10^3$	0.202(4)	0.88891
Fatigued	Charged	SALSA	003 $LiCoO_2$	19.65(2)	$1.15(4) \times 10^3$	0.202(4)	0.90996

[a] COD corresponds to the coefficient of determination $\mathrm{COD} = \sqrt{1 - (\sum_i (I_i^{obs} - I_i^{cal})^2)/(\sum_i (I_i^{obs} - \langle I_i^{obs} \rangle)^2)}$.

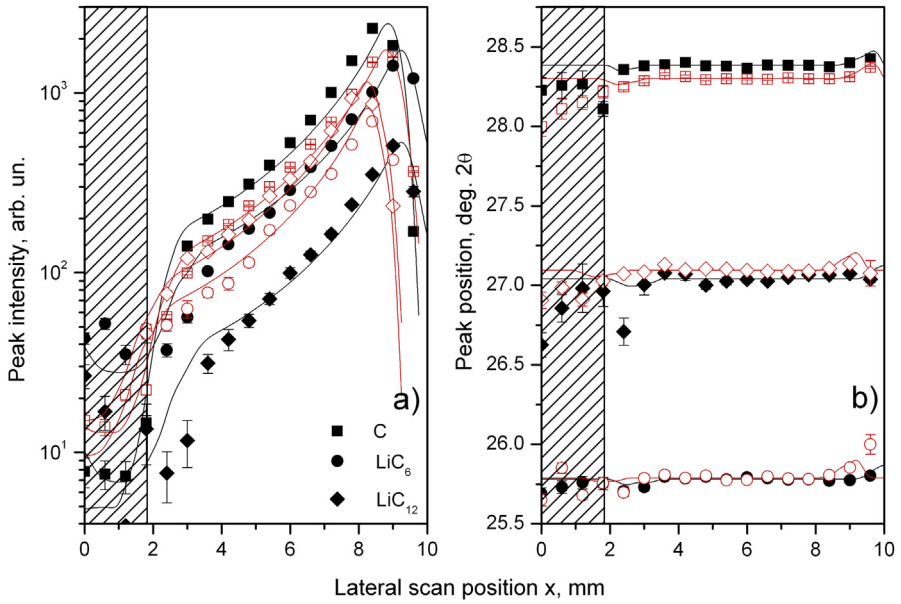

Fig. 3. Intensities (a) and positions (b) of the 001/002 LiC_6/LiC_{12} reflections (charged Li-ion cell) and 002 C (discharged) as extracted from the single profile decomposition of diffraction data on fresh (black) and fatigued (red) batteries collected at SALSA diffractometer ($2 \times 2 \times 20$ $mm^3/sin2\theta$ gauge volume). Solid lines denote model simulations with the parameters listed in Table 1. (For interpretation of the references to color in this figure legend, the reader is referred to the web version of this article.)

discharged state the 003 $LiCoO_2$ reflection of the fatigued cell has been found at significantly lower diffraction angles, corresponding to less lithium content [4].

Two independent spatially-resolved neutron diffraction experiments do not indicate significant inhomogeneities of the lithium distribution in a commercial cylindrical Li-ion cell of the 18650-type (within the limits of experimental accuracy). The obtained reflection intensities and their ratios are in good agreement with previous diffraction data [3,4]. The spatial intensity distribution can be adequately modeled by a single absorption coefficient down to 1 mm^3 gauge volume, when the geometrical boundary conditions are properly taken into account. Therefore, previous neutron tomography data [3], whose 3D reconstruction is shown on the left-hand side in Fig. 5, need to be reconsidered. Accordingly, an attenuation gradient in radial cell direction has been observed for the computed neutron tomography on a cylindrical Li-ion cell of the 18650 type based on data acquired with a polychromatic neutron beam. It shows a change of the attenuation from green color in the middle to yellow at the cell surface, which may be related to a non-uniform distribution of lithium or electrolyte inside the cell. On the other hand, for highly neutron-absorbing media, like the investigated Li-ion cells, the use of a "thermal/cold" neutron spectrum may result in a beam hardening artifact during data reconstruction. This is explained by the fact that neutrons of lower energies are

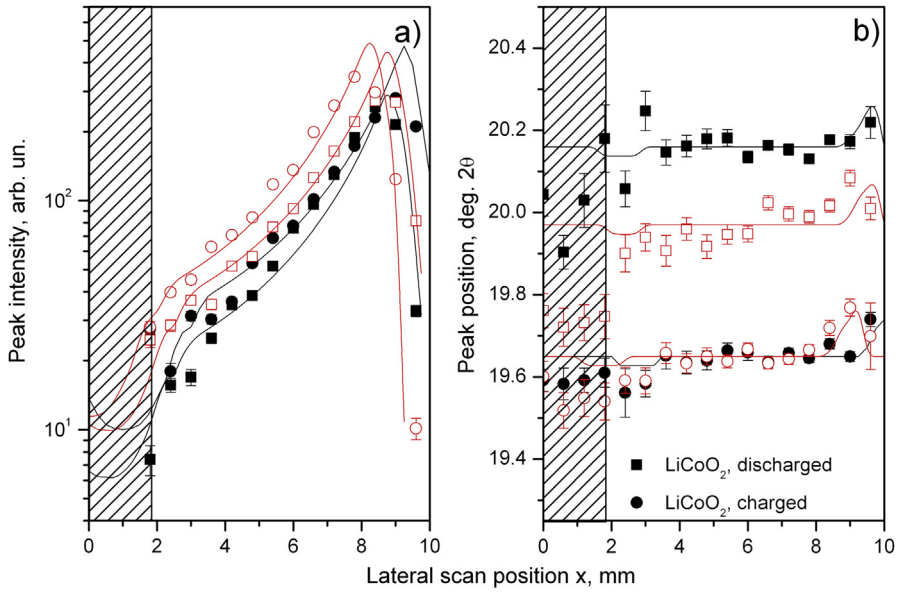

Fig. 4. Intensities (a) and positions (b) of the 003 reflection of $LiCoO_2$ determined using a single profile decomposition of diffraction data on fresh (black) and fatigued (red) cells collected at SALSA diffractometer ($1 \times 1 \times 20$ mm^3 gauge volume). Solid lines denote model calculations with the parameters listed in Table 1. (For interpretation of the references to color in this figure legend, the reader is referred to the web version of this article.)

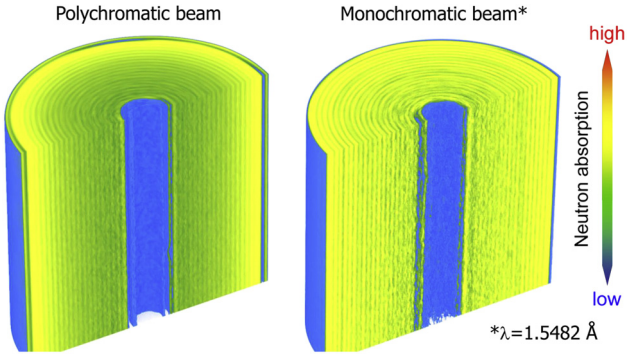

Fig. 5. 3D visualization of the commercial 18650 Li-ion cell (discharged to 3.0 V), reconstructed from neutron radiography based on data acquired using a "white" neutron beam (left) and monochromatic neutrons (right). The reconstructed attenuation coefficients are visualized by assignment of different colors using a consistent color scheme. (For interpretation of the references to color in this figure legend, the reader is referred to the web version of this article.)

more probably absorbed per unit length along the beam path. Thus the neutron energy distribution in the beam is shifted to higher energies after transmission through the sample.

Such an effect may lead to an overestimated neutron attenuation coefficient at the surface compared to the inner part and, accordingly, results in a gradient towards the object center. A so-called beam hardening correction is usually applied in order to correct for this effect during the reconstruction process.

Spatially-resolved neutron diffraction unambiguously indicated a homogeneous distribution of lithium in the polycrystalline electrode materials. Therefore, an independent check of a possible absorption gradient is needed, which is not biased by beam hardening. An appropriate experiment is neutron imaging with monochromatic neutrons, and such an experiment on a discharged Li-ion cell of the same type has been performed at the high-resolution powder diffractometer SPODI [24]. In contrast to the previous setup the 3D reconstruction was performed on the basis of a batch consisting of 400 angular steps over 360° with two projection images of 150 s exposure time each acquired at every projection angle. A custom macro for ImageJ [25] has been applied for a pre-filtering to remove gamma spots and to calculate the average of the multiple projections. The reconstruction has been carried out by Octopus 8.5 [26] with a filtered back projection algorithm. VGStudio Max from Volume Graphics [27] has been used for data visualization, and the corresponding 3D distribution of absorption in false-color representation is shown in Fig. 5, right.

Both 3D tomography reconstruction data sets shown in Fig. 5 are very similar and the resolution in both cases was sufficient to resolve the center pin and the rolled up electrode layers. However the pronounced absorption gradient features observed at ANTARES using a "thermal/cold" neutron spectrum were not confirmed using monochromatic neutron imaging. This would unambiguously point out that the previously observed [3] absorption gradient can be attributed to the artifacts from the beam hardening effect and not to an inhomogeneity of the lithium distribution, which is in agreement with the performed spatially-resolved neutron diffraction experiments.

Overall, the observed experimental evidences conclude the uniformity of the Li distribution in the cell volume, which, in contrast to observations from Ref. [18], is not affected by cell fatigue (at least not on the resolved length scale and over the investigated life time). Spatially-resolved neutron diffraction as well as neutron imaging with monochromatic neutrons (computed neutron tomography) emphasize the importance of neutron methods for non-destructive in operando probing of Li-ion batteries. The conducted experiments successfully show that spatially resolved neutron diffraction is perfectly suited for in operando and post mortem studies of spatial inhomogeneities occurring in Li-ion cells down to the millimeter length scale, and neutron imaging bring this scale down to the range of several μm.

Acknowledgments

This work was supported by Deutsche Forschungsgemeinschaft (Research Collaborative Centre 595 "Electrical Fatigue in Functional Materials").

References

[1] H. Ehrenberg, A. Senyshyn, M. Hinterstein, H. Fuess, in: E.J. Mittermeijer, U. Welzel (Eds.), In Situ Diffraction Measurements: Challenges, Instrumentation, and Examples, Modern Diffraction Methods, vol. 16, Wiley-VCH, Weinheim, 2012, p. 528.
[2] M.A. Rodriguez, D. Ingersoll, S.C. Vogel, D.J. Williams, Electrochem. Sol. State Lett. 7 (1) (2004) A8–A10.
[3] A. Senyshyn, M.J. Mühlbauer, K. Nikolowski, T. Pirling, H. Ehrenberg, J. Power Sources 203 (2012) 126–129.
[4] O. Dolotko, A. Senyshyn, M.J. Mühlbauer, K. Nikolowski, F. Scheiba, H. Ehrenberg, J. Electrochem. Soc. 159 (12) (2012) A2082–A2088.
[5] N. Sharma, V.K. Peterson, J. Power Sources (2012). in press.
[6] N. Sharma, V.K. Peterson, M.M. Elcombe, M. Avdeev, A.J. Studer, N. Blagojevic, R. Yusoff, N. Kamrulzaman, J. Power Sources 195 (2010) 8258–8266.
[7] X.-L. Wang, K. An, L. Cai, Z. Feng, S.E. Nagler, C. Daniel, K.J. Rhodes, A.D. Stoica, H.D. Skorpenske, C. Liang, W. Zhang, J. Kim, Y. Qi, S.J. Harris, Scientific Rep. 2 (2012) 747.
[8] N. Sharma, X. Guo, G. Du, Z. Guo, J. Wang, Z. Wang, V.K. Peterson, J. Am. Chem. Soc. 134 (2012) 7867–7873.
[9] N. Sharma, V.K. Peterson, J. Sol. State Electrochem. 16 (2012) 1849–1856.
[10] L. Liang, S.S. Lee, H.S. Choi, B.-S. Seong, C.-W. Yi, K. Kim, in: 216th Meeting of Electrochemical Society, 4–9 October 2009, Vienna, Austria (2009), p. 549. Conference abstracts 902(8).
[11] C.A. Bridges, X.-G. Sun, J. Zhao, M.P. Paranthaman, S. Dai, J. Phys. Chem. C 116 (2012) 7701–7711.
[12] J.E. Owejan, J.P. Owejan, S.C. DeCaluwe, J.A. Dura, Chem. Mater. 24 (2012) 2133–2140.
[13] M. Kamata, T. Esaka, S. Fujine, K. Yoneda, K. Kanda, J. Power Sources 68 (1997) 459–462.
[14] M. Lanz, E. Lehmann, R. Imhof, I. Exnart, P. Novak, J. Power Sources 101 (2001) 177–181.
[15] D. Goers, M. Holzapfel, W. Scheifele, E. Lehmann, P. Vontobel, P. Novak, J. Power Sources 130 (2004) 221–226.
[16] I. Manke, J. Banhart, A. Haibel, A. Rack, S. Zabler, N. Kardjilov, A. Hilger, A. Melzer, H. Riesemeier, Appl. Phys. Lett. 90 (2007) 214102.
[17] M. Hofmann, R. Gilles, Y. Gao, J.T. Rijssenbeek, M.J. Muehlbauer, J. Electrochem. Soc. 159 (11) (2012) A1827–A1833.
[18] L. Cai, K. An, Z. Feng, C. Liang, S.J. Harris, J. Power Sources 236 (2013) 163–168.
[19] X.-L. Wang, S. Spooner, C.R. Hubbard, J. Appl. Crystallogr. 30 (1998) 52–59.
[20] M. Hofmann, R. Schneider, G.A. Seidl, J. Rebelo-Kommeier, R.C. Wimpory, U. Garbe, H.G. Brokmeier, Physica B 385–386 (2006) 1035–1037.
[21] J.R. Dahn, Phys. Rev. B 44 (1991) 9170–9177.
[22] T. Pirling, G. Bruno, P.J. Withers, Mat. Sci. Eng. A 437 (1) (2006) 139–144.
[23] A. Senyshyn, O. Dolotko, M.J. Mühlbauer, K. Nikolowski, H. Fuess, H. Ehrenberg, J. Electrochem. Soc. 160 (5) (2013) A3198–A3205. http://jes.ecsdl.org/content/160/5/A3198.abstract.
[24] M. Hoelzel, A. Senyshyn, N. Juenke, H. Boysen, W. Schmahl, H. Fuess, Nucl. Instr. Meth. A 667 (2012) 32–37.
[25] http://rsb.info.nih.gov/ij/.
[26] http://www.octopusreconstruction.com.
[27] http://www.volumegraphics.com/products/vgstudiomax/.